WILEY ECOLOGICAL APPLICATIONS

Integrating field and satellite data for spatially-explicit inference on the density of threatened arboreal primates

Journal:	*Ecological Applications*
Manuscript ID	EAP16-0224.R1
Wiley - Manuscript type:	Articles
Date Submitted by the Author:	n/a
Complete List of Authors:	Cavada, Nathalie; Universita degli Studi di Trento, DICAM; MUSE - Museo delle scienze, Tropical biodiversity section Ciolli, Marco; Universita degli Studi di Trento, DICAM Rocchini, Duccio; Fondazione Edmund Mach, Research and innovation centre, Biodiversity and Molecular Ecology Department Barelli, Claudia; MUSE - Museo delle scienze, Tropical biodiversity section Marshall, Andrew; University of York, CIRCLE, Environment Department; Flamingo Land Ltd. Rovero, Francesco; MUSE - Museo delle Scienze, Tropical biodiversity section
Substantive Area:	Statistics and Modeling < Theory < Substantive Area, Spatial Statistics and Spatial Modeling < Statistics and Modeling < Theory < Substantive Area, Endangered Species < Management < Substantive Area, Reserves/Protected Areas < Management < Substantive Area, Remote Sensing < Methodology < Substantive Area, Conservation < Landscape < Substantive Area
Organism:	Mammals < Vertebrates < Animals, Primates < Mammals < Vertebrates < Animals, Plants
Habitat:	Tropical Zone < Terrestrial < Habitat, Rain Forest < Tropical Zone < Terrestrial < Habitat
Geographic Area:	Africa < Geographic Area, East Africa < Africa < Geographic Area
Additional Keywords:	abundance, basal area, GIS, Landsat, primates, remote sensing, spatially explicit models, tropical forest, Udzungwa

Abstract:	Spatially explicit models of animal abundance are a critical tool to inform conservation planning and management. However, they require the availability of spatially diffuse environmental predictors of abundance, which may be challenging especially in complex and heterogeneous habitats. This is particularly the case for tropical mammals, such as non-human primates, that depend on multi-layered and species-rich tree canopy coverage, which is usually measured through a limited sample of

	ground plots. We developed an approach that calibrates remote-sensing imagery to ground measurements of tree density to derive basal area, in turn used as a predictor of primate density based on published models. We applied generalized linear models (GLM) to relate 9.8 ha ground samples of tree basal area to various metrics extracted from Landsat 8 imagery. We tested the potential of this approach for spatial inference of animal density by comparing the density predictions for an endangered colobus monkey, to previous estimates from field transect counts, measured basal area, and other predictors of abundance. The best GLM had high accuracy and showed no significant difference between predicted and observed values of basal area. Our species distribution model yielded predicted primate densities that matched those based on field measurements. Results show the potential of using open-access and global remote sensing data to derive an important predictor of animal abundance in tropical forests and in turn to make spatially explicit inference on animal density. This approach has important, inherent applications as it greatly magnifies the relevance of abundance modeling for informing conservation. This is especially true for threatened species living in heterogeneous habitats where spatial patterns of abundance, in relation to habitat and/or human disturbance factors, are often complex and, management decisions - such as improving forest protection - may need to be focused on priority areas.

Note: The following files were submitted by the author for peer review, but cannot be converted to PDF. You must view these files (e.g. movies) online.

DataS1.csv

Integrating field and satellite data for spatially-explicit inference on the density of threatened arboreal primates

Nathalie Cavada[1,2], Marco Ciolli[1], Duccio Rocchini[3], Claudia Barelli[2], Andrew R. Marshall[4,5], Francesco Rovero[2,6]

[1]DICAM Department of Civil, Environmental and Mechanical Engineering, University of Trento, Trento, Italy.

[2]Tropical Biodiversity Section, MUSE - Museo delle Scienze, Trento, Italy.

[3]Biodiversity and Molecular Ecology Department, Research and Innovation Centre – Fondazione Edmund Mach, San Michele all'Adige, Italy.

[4]CIRCLE, Environment Department, University of York, York, United Kingdom.

[5]Flamingo Land Ltd., Kirby Misperton, North Yorkshire, York, United Kingdom.

[6]Udzungwa Ecological Monitoring Centre, Udzungwa Mountains National Park, Mang'ula, Tanzania.

Correspondence: Nathalie Cavada, DICAM Department of Civil, Environmental and Mechanical Engineering, University of Trento, Via Mesiano 77, 38123 Trento, Italy.
Phone: +393404122810; E-mail: nathalie.cavada@unitn.it

Keywords: abundance; basal area; GIS; Landsat; primates; remote sensing; spatially explicit models; tropical forest; Udzungwa.

Abstract

Spatially explicit models of animal abundance are a critical tool to inform conservation planning and management. However, they require the availability of spatially diffuse environmental predictors of abundance, which may be challenging especially in complex and heterogeneous habitats. This is particularly the case for tropical mammals, such as non-human primates, that depend on multi-layered and species-rich tree canopy coverage, which is usually measured through a limited sample of ground plots. We developed an approach that calibrates remote-sensing imagery to ground measurements of tree density to derive basal area, in turn used as a predictor of primate density based on published models. We applied generalized linear models (GLM) to relate 9.8 ha ground samples of tree basal area to various metrics extracted from Landsat 8 imagery. We tested the potential of this approach for spatial inference of animal density by comparing the density predictions for an endangered colobus monkey, to previous estimates from field transect counts, measured basal area, and other predictors of abundance. The best GLM had high accuracy and showed no significant difference between predicted and observed values of basal area. Our species distribution model yielded predicted primate densities that matched those based on field measurements. Results show the potential of using open-access and global remote sensing data to derive an important predictor of animal abundance in tropical forests and in turn to make spatially explicit inference on animal density. This approach has important, inherent applications as it greatly magnifies the relevance of abundance modeling for informing conservation. This is especially true for threatened species living in heterogeneous habitats where spatial patterns of abundance, in relation to habitat and/or human disturbance factors, are often complex and, management decisions - such as improving forest protection - may need to be focused on priority areas.

Introduction

Species abundance estimation and the identification of factors predicting its variation is a pervasive goal in ecology and conservation biology and it is gaining increasing attention through the emergent potential of spatially explicit modeling (Guisan and Zimmermann 2000, Guisan and Thuiller 2005,

Wulder and Franklin 2006, Anadón et al. 2010). This is particularly true for threatened species living in heterogeneous landscapes, where habitat structure and human disturbance vary according to complex spatial patterns. In these contexts, inference on abundance becomes truly informative only when it accounts for such heterogeneity (Arroyo-Rodríguez and Fahrig 2014). Human-modified landscapes are also expanding in tropical areas, where forest fragmentation, degradation and defaunation strongly affect species viability (Balmford and Whitten 2003, Arroyo-Rodríguez and Fahrig 2014). However, because of limited and substandard data, spatially explicit models are less exploited in tropical areas compared to temperate ones (Cayuela et al. 2009). Thus, integrating the use of field data with remote sensing data represents an advantageous approach to ensure data quality for spatial modeling in these areas (Wilkie and Finn 1996, Proisy et al. 2007).

Remote sensing data (especially Landsat) have been used to investigate several ecological questions, mainly related to land cover change, carbon storage and habitat mapping (Schroeder et al. 2011, Legaard et al. 2015, Mayes et al. 2015, Twongyirwe et al. 2015). However, the resolution and quality of Landsat data do not always adequately represent environmental components that are most important for target species, such as vegetation structure, because optical satellite imagery is not three-dimensional (Hall et al. 1995, Duncanson et al. 2010). Therefore, methods are needed to characterize features of the forest structure that are relevant to target species, particularly for inaccessible areas where Landsat images represent the only feasible option.

In this study, we aimed to derive arboreal primate density from remote sensing estimates of 'tree stem basal area'. Basal area is typically related to canopy cover (Alexander 1971, Farr et al. 1989, Smith et al. 1992), but the two measures are not directly interchangeable (Cade 1997). In particular, mean basal area specifically measures the contribution of each tree to biomass and hence identifies forest structure, succession stage and disturbance. Accordingly, it is a common measure of habitat quality for predicting animal abundance (Braithwaite et al. 1989, Medley 1993, Umapathy and Kumar 2000). This is especially true for non-human primates (Mbora and Meikle 2004, Cristóbal-

Azkarate et al. 2005, Anderson et al. 2007, Struhsaker and Rovero 2007) which are globally threatened and in urgent need of conservation actions (Schipper et al. 2008, Schwitzer et al. 2015). Our specific objectives were to: a) model measured basal area against a combination of different metrics and indices derived from Landsat imagery; b) test the performance of the best-performing model to predict values of basal area outside of the sampled areas; c) use the results to derive a spatial map of population density of the endangered (IUCN 2015) Udzungwa red colobus monkey (*Procolobus gordonorum*), based on previously published density-basal area model; d) compare the modeled primate density to previous predictions from field measurements; e) further refine these estimates using environmental and human predictors.

Materials and Methods

Study area

The Udzungwa Mountains are located in the south-central part of Tanzania and represent the largest mountain bloc in the Eastern Arc Mountains, covering an area larger than 19,000 km^2 (Platts et al. 2011). Closed forest blocs, ranging in size from 12 to over 500 km^2 (Marshall et al. 2010), are interspersed with drier habitats. We focused our study on the forest of Mwanihana, one of the largest forest blocs (150.6 km^2) and under the protection of the Udzungwa Mountain National Park (UMNP) since 1992. Highly variable habitat types are distributed along the altitudinal gradient of the forest ranging from 351 to 2,263 m a.s.l. Deciduous forest is found in the lowland, with semi-deciduous and evergreen forests covering the sub-montane and montane areas, while *Hagenia* and bamboo-dominated forest characterize the upper montane level (Lovett et al. 2006). Woody vegetation density increases with elevation, with the largest trees found at mid elevation, probably a result of human disturbance and tree respiration costs (Marshall et al. 2012).

Vegetation data

We derived field data for tree stems ≥10cm DBH (Diameter at Breast Height; 1.3m) from three sources (Fig. 1): (1) From the Tropical Ecology Assessment and Monitoring Network (TEAM)

(http://www.teamnetwork.org/, dataset ID 0327011905 4443), comprising six vegetation plots of 100 × 100m on a horizontal plane (i.e. adjusted for slope), following a standardized protocol (TEAM Network 2011); (2) 153 vegetation plots of 25 × 25m, sampled along line transects uniformly distributed in the forest (from Barelli et al. 2015); (3) 33 new randomly placed vegetation plots of 25 × 25m, sampled in June-July 2015, stratified according to the predominant habitat gradient from disturbed lowland deciduous to mature montane evergreen forest. All newly-sampled plots were placed in the centre of Landsat pixels for concordance with our remote-sensing imagery. A summary of the vegetation data sets is provided in Data S1.

We obtained a single, cloud free, L8 OLI/TIRS Landsat image (Landsat scene ID LC81670652014299LGN00, courtesy of the U.S. Geological Survey), acquired October 26, 2014.

Primate density data

Density data on the Udzungwa red colobus from across the study area were obtained from an earlier study (Cavada et al. 2016). This study used environmental covariates from the 153 plots established by Barelli et al. (2015) and distance sampling along line transects, to estimate colobus density across the study area. Transect data were modeled as a hierarchical coupled logistic regression, assuming a Poisson distribution for the animal abundance at a transect level. The detection process of the distance sampling was modeled according to a multinomial distribution, assuming a monotonical decrease of the detection probability with the increasing distance of the animal groups from the observer. The influence of a series of environmental and human disturbance covariates was evaluated and incorporated on both the abundance and detection steps in the model. Final density estimates at the plot level were derived from environmental correlates that included mean basal area, elevation and distance from disturbance (i.e. forest edge), that were found to significantly affect the abundance and detectability of the red colobus in the study area.

Analysis

Landsat metrics and vegetation indices

131 To model basal area we first derived various Landsat metrics (Table 1). This began with a Principal
132 Component Analysis (PCA) to extract uncorrelated information from the different spectral bands
133 provided by the Operational Land Imager (OLI) sensor of the Landsat 8 satellite. After applying
134 PCA we further compressed the spectral data applying the Tasseled Cap Transformation (TCT) to
135 represent forest structure (Cohen et al. 1995). We also used a GRASS module (Neteler et al. 2012),
136 modified to derive vegetation-related spectral indices, combining specific bands of the Landsat 8
137 satellite images (Data S2). Such indices enhance the signal related to vegetation, while minimizing
138 background edaphic, solar and atmospheric effects (Jackson and Huete 1991).
139
140 **Model building**
141 To relate field sampled values of basal area to the metrics calculated from the Landsat images, we
142 used all newly-sampled plots, plus a subsample of the TEAM and Barelli et al. (2015) plots. The
143 subsample plots were those showing at least 75% overlap with Landsat pixels (N=115). In each plot
144 we calculated the basal area (BA, m^2) for each sampled tree (DBH ≥10cm) as $BA=\pi*(DBH/2)^2$. We
145 then derived the mean basal area (MBA) for each plot, for use as the response variable (following
146 Barelli et al. (2015) and Cavada et al. (2016)).
147
148 We used generalized linear modeling (GLM) to investigate the relationship between the MBA- field
149 sampled values and the Landsat metrics and indices. Prior to building the models we checked for
150 the presence of collinearity among predictor variables to remove those providing identical
151 information. We thus calculated Variance Inflation Factor (VIF), using a cut off value of 10
152 (Marquardt 1970, Hair et al. 2006, Kennedy 2008) and we retained the uncorrelated predictors P1,
153 P2, RGI, RR, SLAVI. From an Empirical Cumulative Distribution Function (ECDF) of the response
154 variable, we decided to use an inverse Gaussian error distribution for the GLM with an inverse
155 squared link function (Fig. 2).
156

We built models using all the possible combinations of the retained Landsat predictors and we used the Akaike Information Criterion (AIC) to rank the candidate models. We considered those models showing $\Delta AIC<2$ as equivalent (Anderson and Burnham 2002) and defined an average model by determining Akaike weights (w_i) for each of the best models, using the packages 'AICcmodavg' (Mazerolle 2015) and 'MUMin' (Barton 2014) in R version 3.2.1 (R Core Team 2015). For validating the model we randomly split the MBA dataset into two subsets, one for model fitting with 75% of the data (N=109) and one with the remaining 25% of the data (N=37). We then used bootstrapping to verify the goodness of fit of the selected average model: we simulated 1,000 datasets from the subset derived for model fitting (i.e the one considering 75% of the data) and then defined a function that returned the fit-statistic Pearson χ^2. We validated the model by checking the distribution of the residuals for the validation subset. We evaluated model bias by comparing both observed and predicted values, to a null model of mean residual prediction equal to zero, using Wilcoxon's signed rank test (for $\alpha=0.05$).

Predictions: MBA values and RC density

To predict density values for groups of red colobus across the entire Mwanihana forest, we first derived spatially diffused values for MBA from our best fitting averaged model, giving an MBA value for each Landsat pixel in the entire study area. We removed those values of MBA that appeared as outliers in the derived dataset (i.e. $>0.5m^2$). We believed these outliers were found for those pixels where our model was not able to derive realistic MBA values, inside those areas close to forest borders as well as in areas located at high elevation (above 1800 m), where trees are sparse and are replaced by other vegetation (Lovett et al. 2006).

Besides MBA, previous modeling of red colobus group density was most effective using elevation (negative sign) and distance from disturbance/forest edge (negative sign) (Cavada et al. 2016). We therefore calculated spatially diffused values for these variables from a Digital Elevation Model (DEM) and from a shapefile of the forest edge, respectively. We then used a published hierarchical

model (Cavada et al. 2016) to predict primate density across the Mwanihana forest using these two variables and spatially diffused values for MBA derived from our model.

Finally, we verified the accuracy of our approach by comparing the predicted primate density to density estimates in Cavada et al. (2016) for those plots in Barelli et al. (2015) (N=65) that were excluded while building the MBA model (see 'Model building' above). These density estimates were plot-specific values derived from the hierarchical analysis described above, and hence were effectively the only field based and site-specific density estimates that could be used for such validation. We compared observed and predicted values using OP regression (Piñeiro et al. 2008) and we compared the slope and the intercept of the fitted model with the 1:1 line.

Results

After selecting the plots suitable for the analysis, we retained 61 plots from Barelli et al. (2015) and 54 TEAM sub-plots. Adding these to the 33 newly sampled plots, we obtained an overall dataset of 148 plots and their corresponding sampled MBA values. We built models using all the possible combinations of the metrics and indices calculated from the Landsat images, including a null model. We retained six competing models of MBA (Table 2) that were averaged for predictions. The resulting average model retained the first and the second components of the PCA and the indices RGI, RR and SLAVI (Table 3). This model showed adequate fit based on the bootstrap P value based on the Chi-square statistic (P=0.66) and no significant difference between observed and predicted MBA values (W=602, P=0.92). The MBA model failed to derive plausible values in those areas located at high altitudes as well as close to the forest edge (Fig. 3). We obtained a spatially-explicit map of estimated density of red colobus groups across the whole study area, as influenced by the covariates MBA (predicted from our model and with a positive effect), elevation and distance from disturbance (i.e from the forest edge), both with a negative effect, according to the hierarchical model defined in Cavada et al. (2016) (Fig. 4).

209 The OP regression yielded a R^2 of 0.84 attesting the accuracy of the predicted red colobus group
210 density values as derived by using the spatially diffused values for MBA obtained from the GLM
211 analysis (Fig. 5).
212
213 **Discussion**
214 We have successfully predicted and mapped the spatial density of an endangered primate, hence
215 showing how modeling ecologically-relevant predictors of abundance can improve predictions on
216 species distribution (Franklin 1995), across a broad spatial extent. The species' density pattern
217 highlighted in our map is consistent with results in previous studies that were based solely on
218 ground data and hence with limited spatial inference (Struhsaker and Rovero 2007, Barelli et al.
219 2015, Cavada et al. 2016).
220
221 Our best supported models showed high accuracy in predicting MBA values, making it a reliable
222 tool for inference beyond the ground measurement sites, with a good level of confidence and
223 precision. MBA is a highly relevant descriptor of the canopy structure as well as a significant
224 covariate that has emerged in different studies as influential for predominantly arboreal primates
225 (Struhsaker and Rovero 2007, Cavada et al. 2016). As a parameter quantifying forest cover, MBA is
226 also a recognized proxy for habitat degradation and fragmentation (Urquiza-Haas et al. 2007). The
227 best fit model we derived from GLM retained the first two components of the PCA. This fitted the
228 acknowledged evidence that Landsat products are able to discriminate forested habitats, through the
229 information provided by specific spectral channels (Blair and Baumgardner 1977, Jakubauskas
230 1996, Eklundh et al. 2001, Cohen and Goward 2004), in terms of the differential reflectance emitted
231 by the higher strata of the canopy. The information provided by the Landsat sensors can highlight
232 specific vegetation components (Thenkabail et al. 2000, Almeida and De Souza Filo 2004); in fact
233 the bands of the visible spectrum and of the Short-wave Infrared (SWIR) can be correlated with
234 several forest structures, including basal area (Muukkonen and Heiskanen 2005, 2007, Hall et al.
235 2006). The relationship with MBA shown by the first PCA component of our model might be due to

a large presence of trees with great basal area and tall canopy, causing pronounced shadowing which translates in a lower reflectance.

Among the vegetation indices retained by the models, RGI can be interpreted as a proxy of the forest phenology by the time when the Landsat image was acquired. Since such an index provides information on the ratio of red to green reflectance, the positive effect we found on MBA could be due to the contribution the index generally gives in evaluating the size of the tree crowns, which is related to the basal area extent. During that period, a high amount of trees shows indeed a breakdown of green pigments and leaves fade from green to yellow and red (Motohka et al. 2010). The positive effect we found for RR was also confirmed by other studies that found a correlation between the visible and the SWIR band of the Landsat with several physical structures of the forest canopy, including basal area (Muukkonen and Heiskanen 2005, Hall et al. 2006, Tonolli et al. 2011). In addition, the positive relationship we found between MBA and SLAVI index is not surprising given that the index accounts for the sensitivity of the mid-infrared wavelength to the structure of the canopy, especially for heterogeneous forest compositions (Lymburner et al. 2000).

As the main goal of our study, we used the predicted and spatially diffused values of MBA to derive a map of the Udzungwa red colobus density. This matched, at a wider and spatially-diffuse scale, the density estimates found in prior studies (Barelli et al. 2015; Cavada et al. 2016). In particular, it confirmed the red colobus's preference for lower-elevation forest that are close to its edge, variably disturbed and covered with regenerating vegetation, that is recognized as an important food source for the species (Barelli et al. 2015). Densities decreased where MBA values increased, i.e. in the interior and old growth forest parts and at higher elevation. This in turn indicates resilience of the animal to anthropogenic disturbance and again the preference shown by the species for forest edges. Such a counter intuitive density trend, is clearly visualized in the spatially explicit map we obtained. This provides novel indications for the protection of forest areas that are located at the interface with intense anthropogenic activity.

We have confirmed that the use of remote sensing represents a robust tool to improve model performance and to reduce the costs of data collection (He et al. 2015), which implies bypassing the sample size limits associated with field measurements. We stress the importance of carefully evaluating the process regarding the selection of adequate satellite images, given the sensitivity for seasonality shown by some vegetation indices. High resolution images should certainly be preferred when deriving remote-sensing based predictor variables that can be essential to improve predictive species modeling. Nonetheless, the quality of such images can often be poor, due to cloud coverage that hides the underlying canopy, i.e. the carried amount of information is lower than the spectral noise (Woodcock and Strahler 1987, Ricotta et al. 1999). This phenomenon consistently arises in images of tropical mountain forests, since clouds accumulate relatively more in dense forest cover areas due to evapotranspiration (Nagendra and Rocchini 2008). Still, we demonstrated that since high resolution products in some cases cannot be used, medium resolution images like Landsat proved to be an excellent source of data for applications both in the study of tropical forest structure and to develop reliable species distribution models. However, caution is recommended regarding the generalization of our approach, which is mainly relevant to comparable study systems in terms of both habitat and target species characteristics.

Conclusions

Spatially explicit, predictive models of animal abundance can offer a powerful insight on the species status and distribution, helping to identify those sites where urgent intervention is needed in terms of protection and conservation. Overcoming the lack of high resolution and high quality remote sensing products as well as of spatially diffused covariates of abundance is essential, as it can firmly boost the usefulness of species distribution models. By focusing on the endangered Udzungwa red colobus, we showed the potential of this approach to derive accurate spatially diffused estimates of animal density and distribution. This approach is particularly suitable for species for which data availability is incomplete and spatial coverage is heterogeneous, affecting the

capacity of developing site-specific conservation and restoration programs where urgent forest and species protection is needed.

Acknowledgements

We thank the Tanzania Wildlife Research Institute (TAWIRI), Tanzania Commission for Science and Technology (COSTECH), Tanzania National Parks (TANAPA) and the Tanzania Forest Service (TFS) for granting us permissions to collect the new data for the study (Costech Permit No. 2015–44– NA– 2015- 37 to N.C.). The new data collection for this study was funded by Rufford Small Grants Foundation (1106-C to F.R.), and by MUSE-Museo delle Scienze and the University of Trento to N.C. We thank L. Perathoner for providing helpful support and valuable suggestion for the analysis of the Landsat dataset and for the implementation of the GRASS code. R. Laizzer and A. Mwakisoma provided invaluable field assistance. We thank the Tropical Ecology Assessment and Monitoring (TEAM) Network, a collaboration between Conservation International, the Smithsonian Institute and the Wildlife Conservation Society, for providing part of the tree plot dataset; some of these plots were in turn established through the Valuing the Arc programme and in collaboration with J. Lovett, S. Lewis and P. Munishi. We thank H. Little for proof-reading the final version of the manuscript and two anonymous reviewers for their relevant suggestions through the revision process.

References

Alexander, R. R. 1971. Crown Competition Factor (CCF) for Engelmann Spruce in the Central Rocky Mountains. Ed 1971 Forest Service, U.S. Dept. of Agriculture, Rocky Mountain Forest and Range Experiment Station.

Almeida, T. I. R., and C. De Souza Filo. 2004. Principal component analysis applied to feature-oriented band ratios of hyperspectral data: A tool for vegetation studies. International Journal of Remote Sensing 25:5005–5023.

Anadón, J. D., A. Giménez, and R. Ballestar. 2010. Linking local ecological knowledge and habitat modelling to predict absolute species abundance on large scales. Biodiversity and Conservation 19:1443–1454.

Anderson, D. R., and K. P. Burnham. 2002. Avoiding pitfalls when using information-theoretic methods. The Journal of Wildlife Management 66:912–918.

Anderson, J., G. Cowlishaw, and J. M. Rowcliffe. 2007. Effects of forest fragmentation on the abundance of Colobus angolensis palliatus in Kenya's coastal forests. International Journal of Primatology 28:637–655.

Araldi, A., C. Barelli, K. Hodges, and F. Rovero. 2014. Density estimation of the endangered Udzungwa red colobus (Procolobus gordonorum) and other arboreal primates in the Udzungwa Mountains using systematic Distance Sampling. International Journal of Primatology 35:941–956.

Arroyo-Rodríguez, V., and L. Fahrig. 2014. Why is a landscape perspective important in studies of primates? American Journal of Primatology 909:901–909.

Balmford, A., and T. Whitten. 2003. Who should pay for tropical conservation, and how could the costs be met? Oryx 37:238–250.

Barelli, C., R. Mundry, A. Araldi, K. Hodges, D. Rocchini, and F. Rovero. 2015. Modelling primate abundance in complex landscapes: a case study from the Udzungwa Mountains of Tanzania. International Journal of Primatology 36:209-226.

Barton, K. 2014. Multi-model inference. R package MuMIn version 1.10.5, 46.

Blair, B. O., and M. F. Baumgardner. 1977. Detection of the green and brown wave in hardwood canopy covers using multidate, multispectral data from LANDSAT-1. Agronomy Journal 69: 808-811.

Braithwaite, L. W., M. P. Austin, M. Clayton, J. Turner, and A. O. Nicholls. 1989. On predicting the presence of birds in Eucalyptus forest types. Biological Conservation 50:33–50.

Brown, L., J. M. Chen, S. G. Leblanc, and J. Cihlar. 2000. A shortwave infrared modification to the Simple Ratio for LAI retrieval in boreal forests: an image and model analysis. Remote Sensing of Environment 71:16–25.

Cade, B. S. 1997. Comparison of tree basal area and canopy cover in habitat models: subalpine forest. Journal of Wildlife Management 61:326–335.

354 Cavada, N., C. Barelli, M. Ciolli, and F. Rovero. 2016. Primates in human-modified and fragmented
355 landscapes: the conservation relevance of modelling habitat and disturbance factors in density
356 estimation. Plos One 11:e0148289.

357 Cayuela, L., D. Golicher, A. Newton, H. Kolb, F. S. de Alburquerque, E. J. M. M. Arets, J. R. M.
358 Alkemade, and A. M. Pérez. 2009. Species distribution modelling in the tropics: problems,
359 potentialities, and the role of biological data for effective species conservation. Tropical
360 Conservation Science 2:319–352.

361 Chen, J. M. 1996. Evaluation of vegetation indices and a modified Simple Ratio for boreal
362 applications. Canadian Journal of Remote Sensing 22:1–21.

363 Cohen, W. B. and S. N. Goward. 2004. Landsat's role in ecological applications of Remote Sensing.
364 BioScience 54:535–545.

365 Cohen, W. B., T. A. Spies, and M. Fiorella 1995. Estimating the age and structure of forests in a
366 multi-ownership landscape of western Oregon, U.S.A. International Journal of Remote Sensing
367 16:721–746.

368 Coops, N. C., M. Johnson, M. A. Wulder, and J. C. White 2006. Assessment of QuickBird high
369 spatial resolution imagery to detect red attack damage due to mountain pine beetle infestation.
370 Remote Sensing of Environment 103:67–80.

371 Cristóbal-Azkarate, J., J. J. Veà, N. Asensio, and E. Rodríguez-Luna. 2005. Biogeographical and
372 floristic predictors of the presence and abundance of mantled howlers (Alouatta palliata
373 mexicana) in rainforest fragments at Los Tuxtlas, Mexico. American Journal of Primatology
374 67:209–222.

375 Duncanson, L. I., K. O. Niemann, and M. A. Wulder. 2010. Integration of GLAS and Landsat TM
376 data for aboveground biomass estimation. Canadian Journal of Remote Sensing 36:129–141.

377 Eklundh, L., L. Harrie, and A. Kuusk. 2001. Investigating relationships between Landsat ETM+
378 sensor data and leaf area index in a boreal conifer forest. Remote Sensing of Environment
379 78:239–251.

380 Farr, W. A., D. J. DeMars, and J. E. Dealy. 1989. Height and crown width related to diameter for
381 open-grown western hemlock and Sitka spruce. Canadian Journal of Forest Research 19:
382 1203–1207.

383 Franklin, J. 1995. Predictive vegetation mapping: geographic modelling of biospatial patterns in
384 relation to environmental gradients. Progress in Physical Geography 19:474–499.

385 Gamon, J. A., and J. S. Surfus. 1999. Assessing leaf pigment content and activity with a
386 reflectometer. New Phytologist 143:105–117.

387 Gitelson, A. A., Y. J. Kaufman, and M. N. Merzlyak. 1996. Use of a green channel in remote
388 sensing of global vegetation from EOS-MODIS. Remote Sensing of Environment 58:289–298.

389 Guisan, A. and W. Thuiller. 2005. Predicting species distribution: offering more than simple habitat
390 models. Ecology Letters 8:993–1009.

391 Guisan, A., and N. E. Zimmermann. 2000. Predictive habitat distribution models in ecology.
392 Ecological Modelling 135:147–186.

393 Hair, J. F., B. Black, B. Babin, B., R. E. Anderson, and R. L. Tatham. 2006. Multivariate Data
394 Analysis 6th ed. Prentice Hall.

395 Hall, F. G., Y. E. Shimabukuro, and K. Huemmrich. 1995. Remote sensing of forest biophysical
396 structure using mixture decomposition and geometric reflectance models. Ecological
397 Applications 5:993–1013.

398 Hall, R. J., R. S. Skakun, E. J. Arsenault, and B. S. Case. 2006. Modelling forest stand structure
399 attributes using Landsat ETM+ data: application to mapping of aboveground biomass and
400 stand volume. Forest Ecology and Management 225:378–390.

401 Hardinsky, M. A., V. Klemas, and R. M. Smart. 1983. The influence of soil salinity, growth form
402 and leaf moisture on the spectral radiance of Spartina alterniflora canopies. Photogrammetric
403 Engineering and Remote Sensing 48:77-84.

404 He, K. S., B. A. Bradley, A. F. Cord, D. Rocchini, M. N. Tuanmu, S. Schmidtlein, W. Turner, M.
405 Wegmann, and N. Pettorelli. 2015. Will remote sensing shape the next generation of species
406 distribution models? Remote Sensing in Ecology and Conservation 1:4-18.

407 Hédl, R., M. Svátek, M. Dančák, A. W. Rodzay, A. B. Salleh, and A. S. Kamariah. 2009. A new
408 technique for inventory of permanent plots in tropical forests: a case study from lowland
409 dipterocarp forest in Kuala Belalong, Brunei darussalam. Blumea: Journal of Plant Taxonomy
410 and Plant Geography 54:124–130.

411 IUCN. 2015. The IUCN Red List of Threatened Species. Version 2015-4. <www.iucnredlist.org>.
412 Downloaded on 08 March 2016.

413 Jackson, R. D., and A. R. Huete. 1991. Interpreting vegetation indices. Preventive Veterinary
414 Medicine 11:185–200.

415 Jakubauskas, M. E. 1996. Thematic mapper characterization of lodgepole pine seral stages in
416 Yellowstone National Park, USA. Remote Sensing of Environment 56:118–132.

417 Jordan, C. F. 1969. Derivation of leaf-area index from quality of light on the forest floor. Ecology
418 50:663–666.

419 Kennedy, P. 2008. A Guide to Econometrics 6th ed. Wiley-Blackwell.

420 Legaard, K. R., S. A. Sader, and E. M. Simons-Legaard. 2015. Evaluating the impact of abrupt
421 changes in forest policy and management practices on landscape dynamics: analysis of a
422 Landsat image time series in the Atlantic Northern Forest. Plos One 10:e0130428.

423 Lovett, J. C., A. R. Marshall, and J. Carr. 2006. Changes in tropical forest vegetation along an
424 altitudinal gradient in the Udzungwa Mountains National Park, Tanzania. African Journal of
425 Ecology 44:478-490.

426 Lymburner, L., P. Beggs, and C. Jacobson. 2000. Estimation of canopy-average surface-specific leaf
427 area using Landsat TM data. Photogrammetric Engineering & Remote Sensing 66:183–191.

428 Marquardt, D. W. 1970. Generalized inverses, Ridge regression, biased linear estimation, and
429 nonlinear estimation. Technometrics 12:591–612.

Marshall, A. R., H. I. O. Jørgensbye, F. Rovero, P. J. Platts, P. C. L. White, and J. C. Lovett. 2010. The species-area relationship and confounding variables in a threatened monkey community. American Journal of Primatology 72:325–336.

Marshall, A. R., S. Willcock, P. J. Platts, J. C. Lovett, A. Balmford, N. D. Burgess, J. E. Latham, P. K. T. Munishi, R. Salter, D. D. Shirima, and S. L. Lewis. 2012. Measuring and modelling above-ground carbon and tree allometry along a tropical elevation gradient. Biological Conservation 154:20–33.

Mayes, M. T., J. F. Mustard, and J. M. Melillo. 2015. Forest cover change in Miombo Woodlands: modelling land cover of African dry tropical forests with linear spectral mixture analysis. Remote Sensing of Environment 165:203–215.

Mazerolle, M. J. 2015. R package " AICcmodavg " Model selection and multimodel inference based on (Q)AIC(c).

Mbora, D. N. M., and D. B. Meikle. 2004. Forest fragmentation and the distribution, abundance and conservation of the Tana river red colobus (Procolobus rufomitratus). Biological Conservation 118:67–77.

Medley, K. E. 1993. Primate conservation along the Tana River, Kenya: an examination of the forest habitat. Conservation biology **7**:109–121.

Motohka, T., K. N. Nasahara, H. Oguma, and S. Tsuchida. 2010. Applicability of Green-Red Vegetation index for Remote Sensing of vegetation phenology. Remote Sensing 2:2369–2387.

Muukkonen, P., and J. Heiskanen. 2005. Estimating biomass for boreal forests using ASTER satellite data combined with standwise forest inventory data. Remote Sensing of Environment 99:434–447.

Muukkonen, P., and J. Heiskanen. 2007. Biomass estimation over a large area based on standwise forest inventory data and ASTER and MODIS satellite data: A possibility to verify carbon inventories. Remote Sensing of Environment 107:617–624.

Nagendra, H., and D. Rocchini. 2008. High resolution satellite imagery for tropical biodiversity studies: The devil is in the detail. Biodiversity and Conservation 17:3431–3442.

Nemani, R., L. Pierce, S. Running, and L. Band. 1993. Forest ecosystem processes at the watershed scale: sensitivity to remotely-sensed Leaf Area Index estimates. International Journal of Remote Sensing 14:2519–2534.

Ota, T., O. Ahmed, S. Franklin, M. Wulder, T. Kajisa, N. Mizoue, S. Yoshida, G. Takao, Y. Hirata, N. Furuya, T. Sano, S. Heng, and M. Vuthy. 2014. Estimation of airborne Lidar-derived tropical forest canopy height using Landsat time series in Cambodia. Remote Sensing 6:10750–10772.

Piñeiro, G., S. Perelman, J. P. Guerschman, and J. M. Paruelo. 2008. How to evaluate models: observed vs. predicted or predicted vs. observed? Ecological Modelling 216:316–322.

Platts, P. J., N. D. Burgess, R. E. Gereau, J. C. Lovett, A. R. Marshall, C. J. Mc Clean, P. K. E. Pellikka, R. D. Swetnam, and R. Marchant. 2011. Delimiting tropical mountain ecoregions for conservation. Environmental Conservation 38:312–324.

Proisy, C., P. Couteron, and F. Fromard. 2007. Predicting and mapping mangrove biomass from canopy grain analysis using Fourier-based textural ordination of IKONOS images. Remote Sensing of Environment 109:379–392.

R Core Team. 2015. R: A language and environment for statistical computing. R Foundation for Statistical Computing, Vienna, Austria. URL https://www.R-project.org/.

Ricotta, C., G. C. Avena, and F. Volpe. 1999. The influence of principal component analysis on the spatial structure of a multispectral dataset. International Journal of Remote Sensing 20:3367–3376.

Rouse, J. W., R. H. Haas, J. A. Schell, W. D. Deering, and J. C. Harlan. 1974. Monitoring the vernal advancement and retrogradation (greenwave effect) of natural vegetation. Technical report, NASA, United States.

Schipper, J., et al. 2008. The status of the world's land and marine mammals: diversity, threat, and knowledge. Science 322:225–230.

Schroeder, T. A., M. A. Wulder, S. P. Healey, and G. G. Moisen. 2011. Mapping wildfire and clearcut harvest disturbances in boreal forests with Landsat time series data. Remote Sensing of Environment 115:1421–1433.

Schwitzer, C., R. A. Mittermeier, A. B. Rylands, F. Chiozza, E. A. Williamson, J. Wallis, and Cotton, A., editors. 2015. Primates in Peril: The World's 25 Most Endangered Primates 2014-2016. IUCN SSC Primate Specialist Group (PSG), International Primatological Society (IPS), Conservation International (CI), and Bristol Zoological Society, Arlington, VA. iv+93pp.

Smith, W. R., R. M. Farrar Jr., P. A. Murphy, J. L. Yeiser, R. S. Meldahl, and J. S. Kush. 1992. Crown and basal area relationships of open-grown southern pines for modelling competition and growth. Canadian Journal of Forest Research 22:341–347.

Steel, R. I. 2012. The effects of habitat parameters on the behavior, ecology, and conservation of the Udzungwa red colobus monkey (Procolobus gordonorum). Graduate School of Duke University PhD thesis, Department of Biological Anthropology and Anatomy, Duke University.

Struhsaker, T. T., and F. Rovero. 2007. Vegetative predictors of primate abundance: utility and limitations of a fine-scale analysis. American Journal of Primatology 69:1242–1256.

TEAM Network. 2011. Terrestrial vertebrate protocol implementation manual, v. 3.1. Tropical Ecology, Assessment and Monitoring Network, Center for applied biodiversity science, Conservation International, Arlington, VA, USA.

Thenkabail, P. S., R. B. Smith, and E. De Pauw. 2000. Hyperspectral vegetation indices and their relationships with agricultural crop characteristics. Remote Sensing of Environment 71:158–182.

Tonolli, S., M. Dalponte, M. Neteler, M. Rodeghiero, L. Vescovo, and D. Gianelle. 2011. Fusion of airborne LiDAR and satellite multispectral data for the estimation of timber volume in the Southern Alps. Remote Sensing of Environment 115:2486–2498.

Twongyirwe, R., M. Bithell, K. S. Richards, and W. G. Rees. 2015. Land use policy three decades of forest cover change in Uganda' s Northern Albertine Rift Landscape. Land Use Policy 49: 236–251.

Umapathy, G., and A. Kumar. 2000. The occurrence of arboreal mammals in the rain forest fragments in the Anamalai Hills, South India. Biological Conservation 92:311–319.

Urquiza-Haas, T., P. M. Dolman, and C. A. Peres. 2007. Regional scale variation in forest structure and biomass in the Yucatan Peninsula, Mexico: effects of forest disturbance. Forest Ecology and Management 247:80–90.

Vescovo, L., and D. Gianelle. 2008. Using the MIR bands in vegetation indices for the estimation of grassland biophysical parameters from satellite remote sensing in the Alps region of Trentino (Italy). Advances in Space Research 41:1764–1772.

Wilkie, D. S., and J. T. Finn. 1996. Remote sensing imagery for natural resources monitoring: a guide for first-time users. Columbia University Press.

Woodcock, C. E., and A. H. Strahler. 1987. The factor of scale in remote sensing. Remote Sensing of Environment 21:311–332.

Wulder, M. A., and S. E. Franklin. 2006. Understanding forest disturbance and spatial pattern, Remote Sensing and GIS approaches. CRC Press.

549 **Tables**
550

551 **Table 1.** Vegetation indices extracted from a Landsat 8 image for comparison to ground sampled
552 measures of mean basal area (MBA).

Index	Algorithm	Description	References
Simple Ratio (**SR**)	$SR = \rho_{nir}/\rho_{red}$	Index related to changes in the amount of green vegetation; reduces the effect of atmosphere and topography.	(Jordan 1969)
Corrected Simple Ratio (**SRC**)	$SRC = SR\ (1-((\rho_{mir} - \rho_{mir\ min})/(\rho_{mir\ max} - \rho_{mir\ min}))$	Linearizes the relationships with parameters, accounting for MIR band.	(Brown et al. 2000)
Normalized Difference Vegetation Index (**NDVI**)	$NDVI = (\rho_{nir} - \rho_{red})/(\rho_{nir} + \rho_{red})$	Estimates the amount of vegetation, it assumes values that are normalized for the amount of incident radiation.	(Rouse et al. 1974)
Corrected Normalized Difference Vegetation Index (**NDVIC**)	$NDVIC = NDVI\ (1-((\rho_{mir} - \rho_{mir\ min})/(\rho_{mir\ max} - \rho_{mir\ min})$	Linearizes the relationships with parameters, accounting for MIR band	(Nemani et al. 1993)
Modified Simple Ratio (**MSR**)	$MSR = (\rho_{nir}/\rho_{red} - 1)/((\rho_{nir}/\rho_{red})^{1/2} + 1)$	Linearizes the	(Chen 1996)

		relationship between the index and biophysical parameters	
Reflectance Ratio (**RR**)	$RR = \rho_{mir} / \rho_{red}$	Substitutes NIR band in SR with MIR band, which is more sensitive in distinguishing complex and stratified forest structures	(Tonolli et al. 2011)
Normalized Difference Water Index (**NDWI**)	$NDWI = (\rho_{nir} - \rho_{mir})/(\rho_{nir} + \rho_{mir})$	Sensitive to vegetation water	(Hardinsky et al. 1983)
Specific Leaf Area Vegetation Index (**SLAVI**)	$SLAVI = \rho_{nir}/(\rho_{red} + \rho_{mir})$	Estimates Specific Leaf Area	(Lymburner et al. 2000)
Red Green Ratio (**RGR**)	$RGR = \rho_{red}/\rho_{green}$	Sensitive to different foliar pigments	(Gamon and Surfus 1999)
Red Green Index (**RGI**)	$RGI = (\rho_{green} - \rho_{red})/(\rho_{green} + \rho_{red})$	Normalization of RGR results	(Coops et al. 2006)
Green Normalized Difference Vegetation Index (**GNDVI**)	$GNDVI = (\rho_{nir} - \rho_{green})/(\rho_{nir} + \rho_{green})$	Estimates the amount of green vegetation, exploiting the green channel, sensitive to chlorophyll	(Gitelson et al. 1996)
Normalized Canopy Index (**NCI**)	$NCI = (\rho_{mir} - \rho_{green})/(\rho_{mir} + \rho_{green})$	Linearizes the relationships with parameters, accounting for MIR	(Vescovo and Gianelle 2008)

		and green bands	
Tasseled Cap Angle (**TCA**)	TCA = arctan(TCG/TCB)	Index based on the angle formed by brightness (TCB) and greenness (TCG) in the vegetation plane, calculated from TCT (Tasseled Cap Trans-formation)	(Powell et al. 2010)

572 **Table 2.** Akaike Information Criterion (AIC) value for high ranked models (ΔAIC<2) of mean basal
573 area (MBA) modeled as a function of predictors derived from a Landsat 8 image.

Model	AIC	ΔAIC
MBA~P1+RGI	-620.70	0
MBA~P1+RGI+RR	-619.89	0.81
MBA~P1+SLAVI	-619.46	1.24
MBA~P1	-619.097	1.607
MBA~P1+P2+RGI	-619.096	1.609
MBA~P1+RR+SLAVI	-618.98	1.72

574 P1=First component of the Principal Component Analysis; P2= Second component of the Principal
575 Component Analysis; RGI=Red Green Index; RR=Red Ratio; SLAVI=Specific Leaf Area
576 Vegetation Index.
577
578
579
580
581
582
583
584
585
586
587
588
589
590
591

592 **Table 3.** Estimates and standard errors for the parameters retained in the averaged model for mean
593 basal area (MBA) modeled as a function of metrics and indices extracted from a Landsat 8 image.

Model-averaged coefficients	Estimate	SE	p
P1	-37.92	19.61	0.05
RGI	31.71	15.43	0.04
RR	19.40	16.45	0.2
SLAVI	27.09	16.18	0.09
P2	18.15	24.64	0.4

594 P1=First component of the Principal Component Analysis; P2= Second component of the Principal
595 Component Analysis; RGI=Red Green Index; RR=Red Ratio; SLAVI=Specific Leaf Area
596 Vegetation Index.
597
598
599
600
601
602
603
604
605
606
607
608
609
610
611
612

613 **Figures**

614

615

616

617

618

619

620

621

622

623

624

625

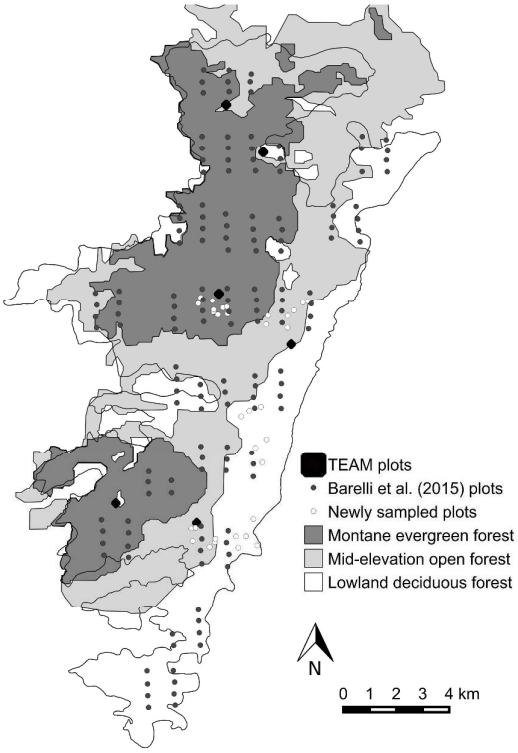

626 **Fig. 1.** Map of Mwanihana forest in the Udzungwa Mountains of Tanzania showing the distribution

627 of three vegetation plots data-sets used to derive basal area.

628

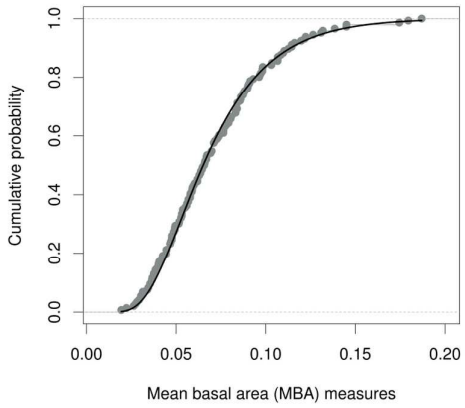

Fig. 2. Empirical cumulative distribution function of ground sampled measures of mean basal area (MBA, gray dots) collected at tree plots in Mwanihana forest, Udzungwa Mountains, Tanzania. The black line shows the fit of the theoretical inverse Gaussian distribution.

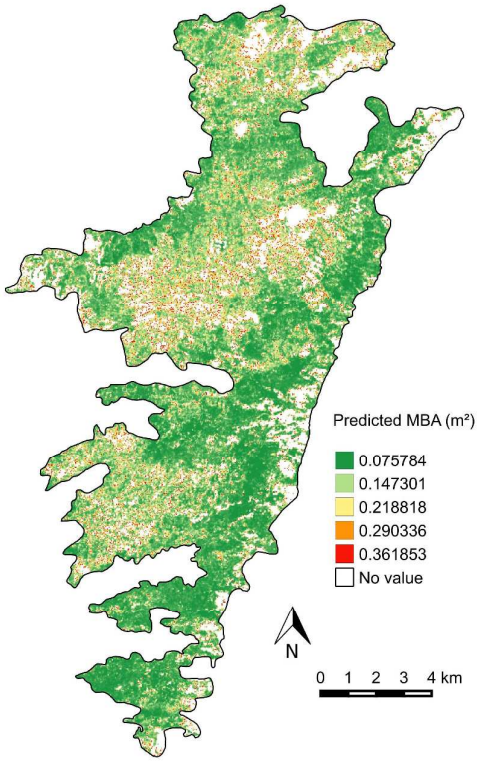

Fig. 3. Predicted values of mean basal area (MBA) across Mwanihana forest using the average model of ground sampled values versus Landsat 8 metrics. White areas show pixels where the model failed to predict plausible values of MBA (i.e. <0.5m^2).

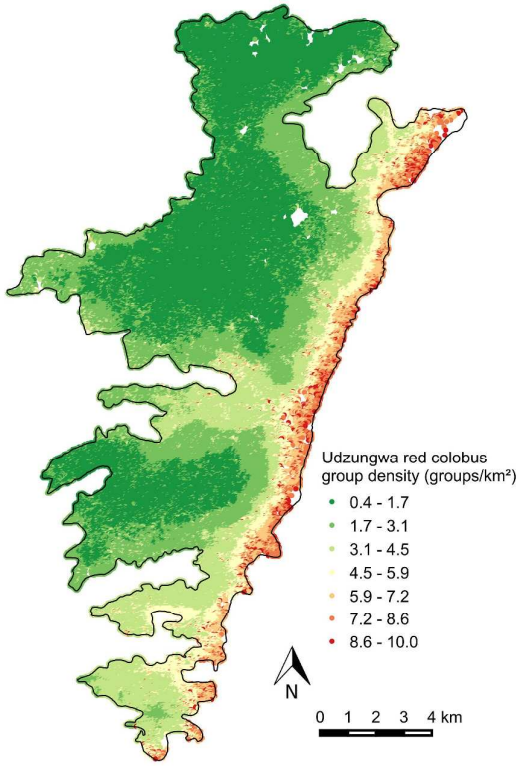

Fig. 4. Predicted Udzungwa red colobus group density in Mwanihana forest using a species density model (Cavada et al. 2016) derived from remotely sensed mean basal area.

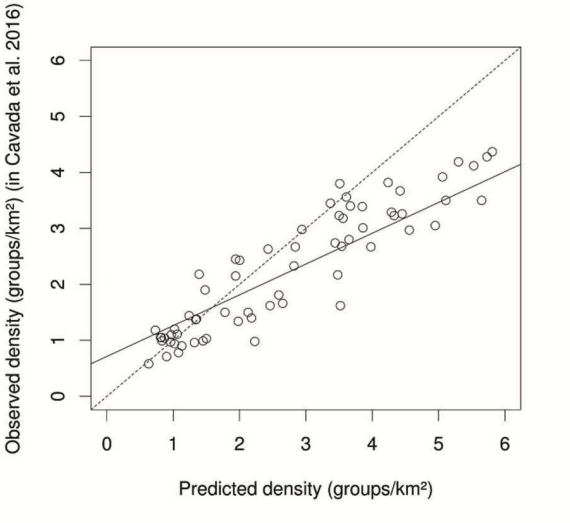

Fig. 5. Linear regression (dotted line) of observed versus predicted values of Udzungwa red colobus density (groups/km^2) among test vegetation plots (N=66). A 1:1 relationship is indicated by the solid line.

711 **Supporting information**

712 **Data S1.** Summary of the dataset regarding the field sampled vegetation

713 **Data S2.** Code for the GRASS 7.0 module that was implemented to derive a series of vegetation

714 indices, combining specific bands of a Landsat 8 image.

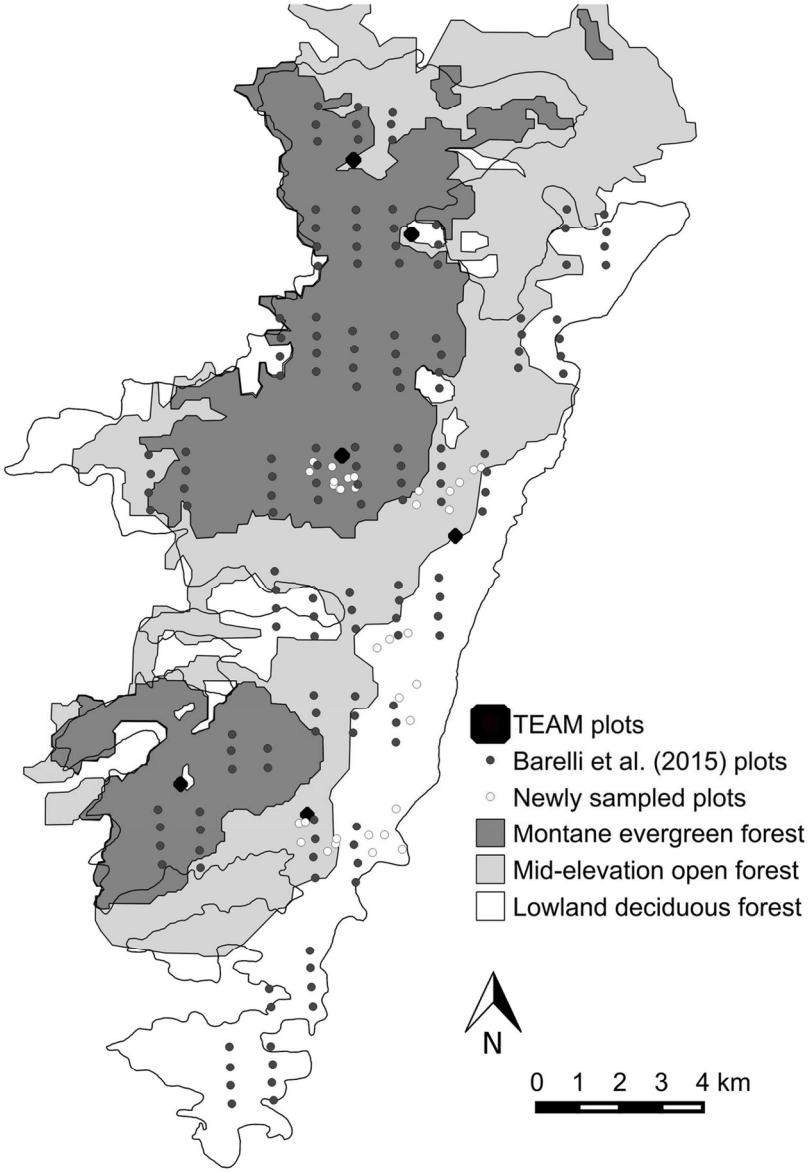

Fig. 1. Map of Mwanihana forest in the Udzungwa Mountains of Tanzania showing the distribution of three vegetation plots data-sets used to derive basal area.

107x152mm (300 x 300 DPI)

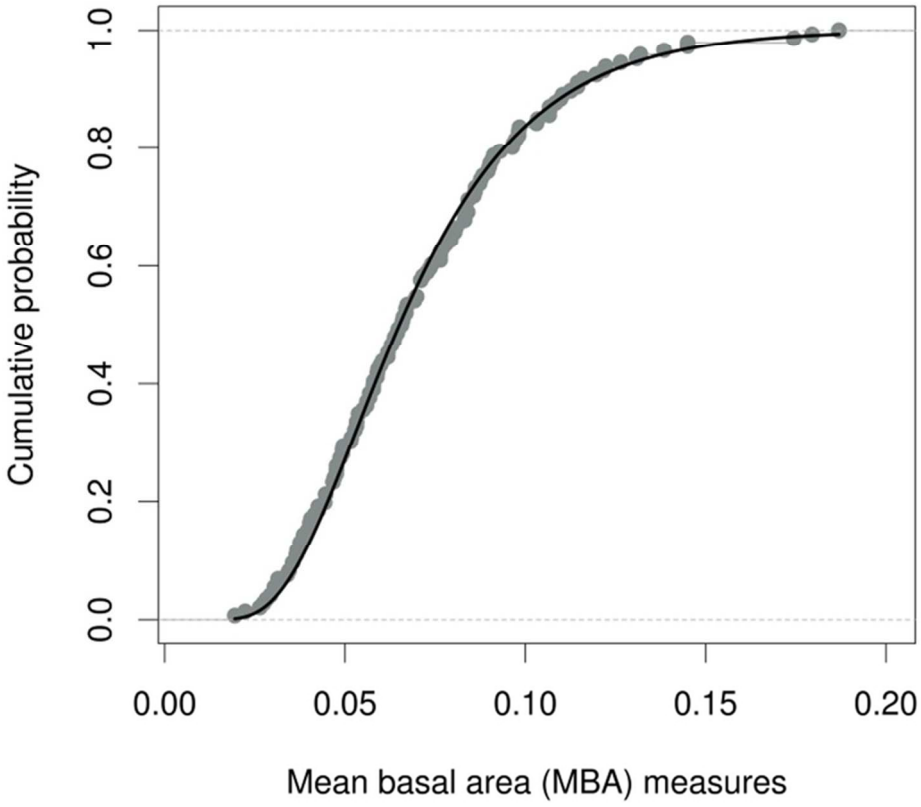

Fig. 2. Empirical cumulative distribution function of ground sampled measures of mean basal area (MBA, gray dots) collected at tree plots in Mwanihana forest, Udzungwa Mountains, Tanzania. The black line shows the fit of the theoretical inverse Gaussian distribution.

70x70mm (300 x 300 DPI)

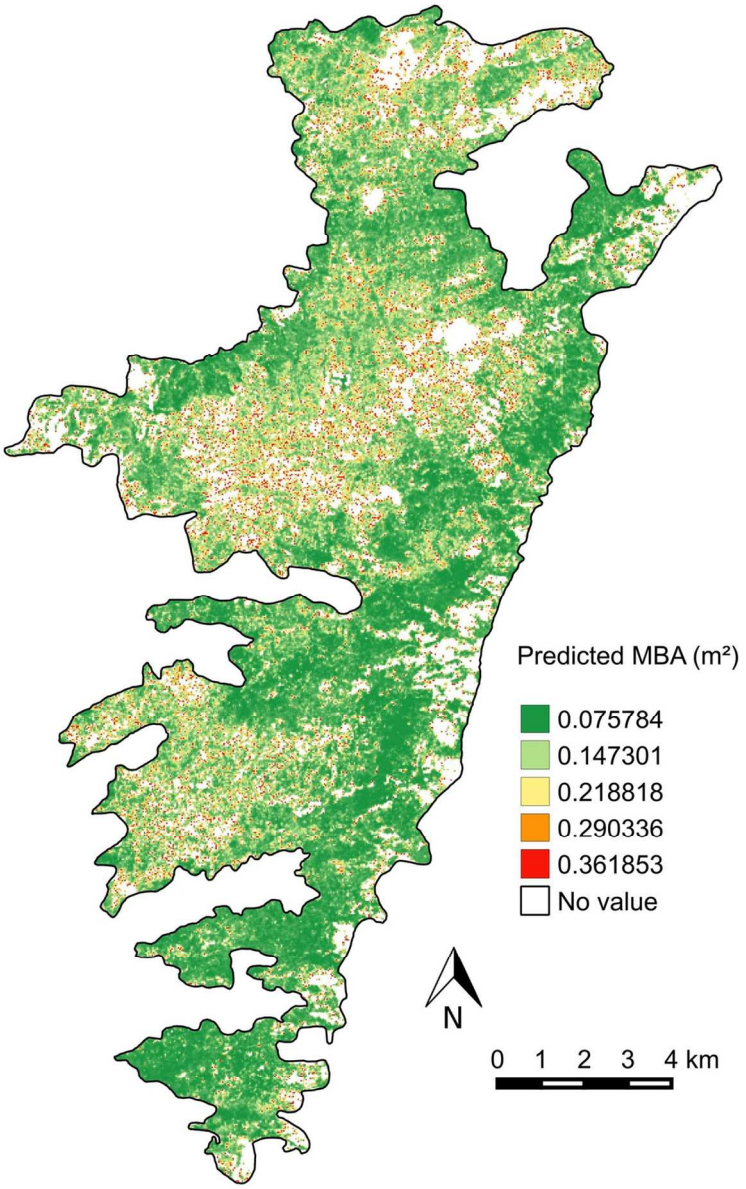

Fig. 3. Predicted values of mean basal area (MBA) across Mwanihana forest using the average model of ground sampled values versus Landsat 8 metrics. White areas show pixels where the model failed to predict plausible values of MBA (i.e. <0.5m2).

107x152mm (300 x 300 DPI)

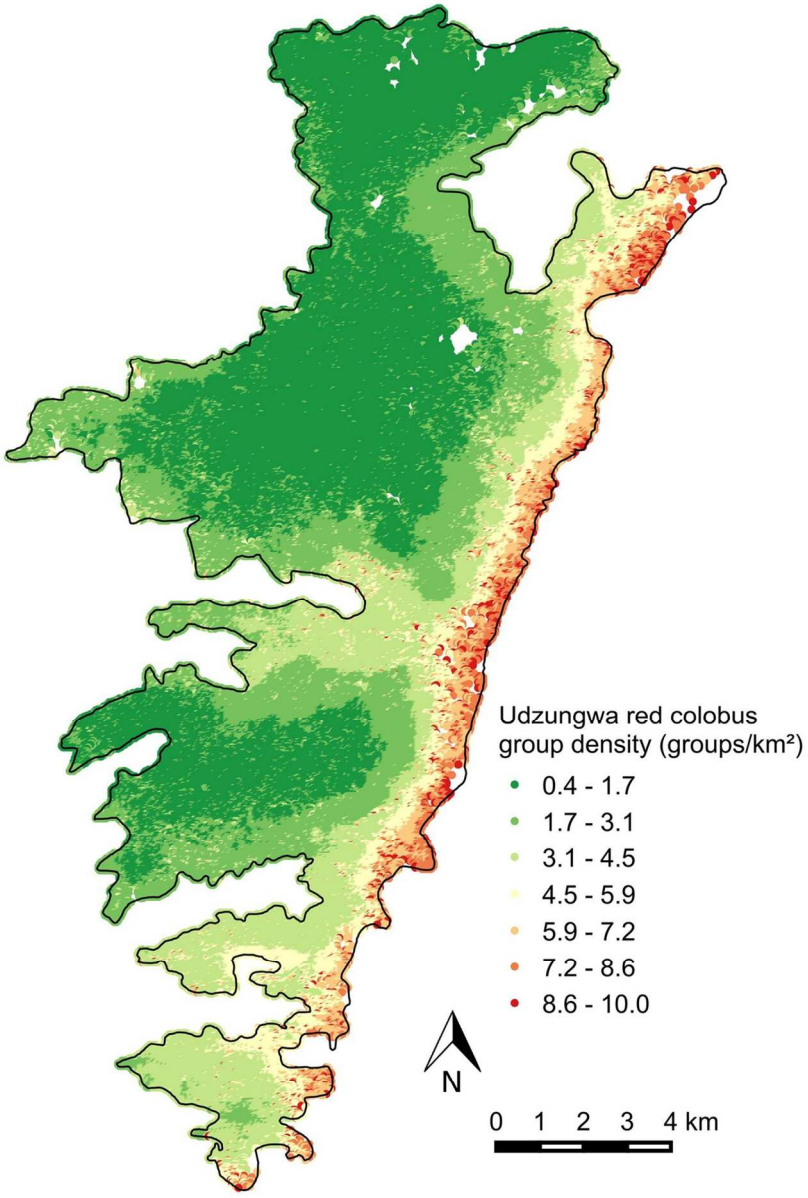

Fig. 4. Predicted Udzungwa red colobus group density in Mwanihana forest using a species density model (Cavada et al. 2016) derived from remotely sensed mean basal area.

107x152mm (300 x 300 DPI)

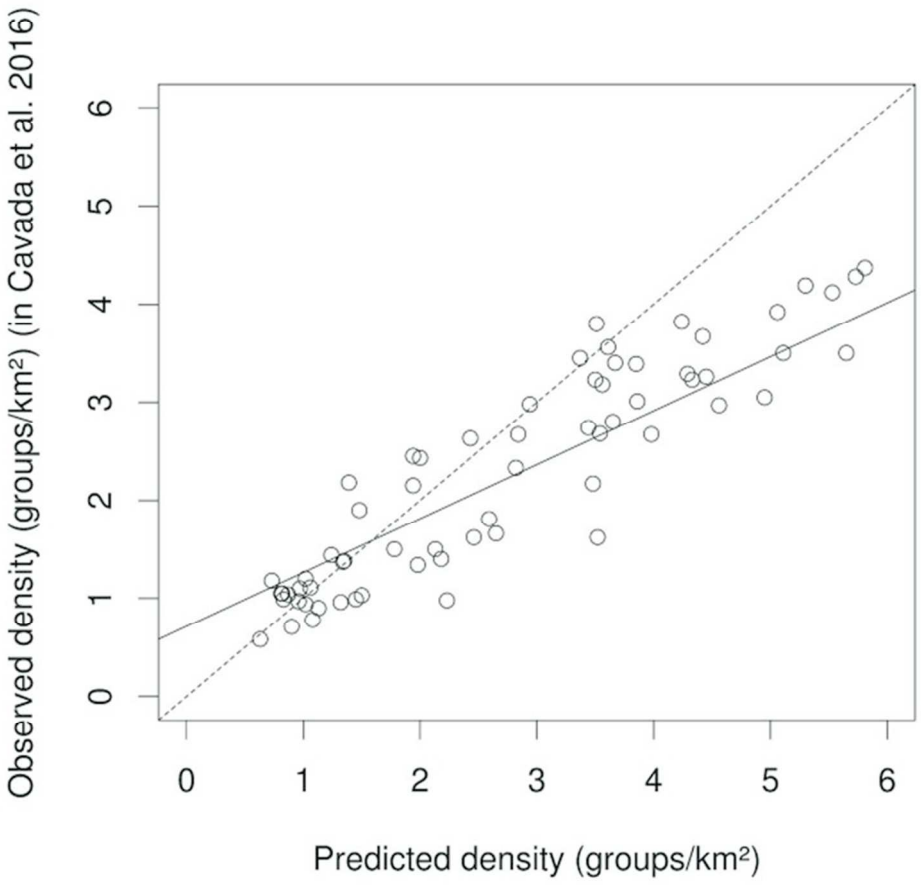

Fig. 5. Linear regression (dotted line) of observed versus predicted values of Udzungwa red colobus density (groups/km2) among test vegetation plots (N=66). A 1:1 relationship is indicated by the solid line.

76x76mm (300 x 300 DPI)

S1 Metadata

Data set: ID for the data set source

DBH: Diameter at breast height, measured for all the tree stems having diameter >=10cm

Basal area: $BA=\pi*(DBH/2)^2$

Climber: visually estimated coverage of climbers on trees as proportion of volume of the canopy, using 5 classes (0,25,50,75,100%).

Canopy: visually estimated extent of canopy cover,using 5 classes (0,25,50,75,100%)

```
#!/usr/bin/env python
#%module
#% description: Calculates vegetation indices for Landsat TM/ETM+/OLI spectral
bands
#% keywords: landsat, vegetation, indices, spectral, bands
#%end

#%option
#% key: band_prefix
#% type: string
#% gisprompt: old,cell,raster
#% description: Base name of input raster bands or a raster band map
#% required: yes
#%end
#%option
#% key: indices_prefix
#% type: string
#% description: Prefix for output raster indices maps
#% answer: spectral
#% required : yes
#%end
#%flag
#%  key: t
#%  description: Use bands for LANDSAT-4,5,7 (TM/ETM+)
#%END
#%flag
#%  key: o
#%  description: Use bands for LANDSAT-8 (OLI)
#%END
#%flag
#%  key: c
#%  description: Calculates also Cap Tassellation Indices
#%END
#%option
#% key: tc_prefix
#% type: string
#% gisprompt: old,cell,raster
#% description: If c flac: base name of input Tasselled Cap or a Tasselled Cap
map
#% required: no
#%end
#%Option
#% key: sensor
#% type: string
#% required: yes
#% multiple: no
#% options: LANDSAT-4;5;7 (TM/ETM+),LANDSAT-8 (OLI)
#% description: Use bands for sensor
#% answer: LANDSAT-8 (OLI)
#%End


import os, sys, shutil
import os.path, re
import grass.script as g


def main():

    #r.mapcalc float coercing with integer input
```

```
    #(dn_B6-dn_B4)/(dn_B6+dn_B4)
    #1.0*(dn_B6-dn_B4)/(dn_B6+dn_B4)
    #(1.0*dn_B6-1.0*dn_B4)/(1.0*dn_B6+1.0*dn_B4)
    #(float(dn_B6)-float(dn_B4))/(float(dn_B6)+float(dn_B4))

    # define indices formulas

    # RR: SWIR/Red reflectance ratio
    rr_expr = '%(outpref)s_rr =1.0* %(mir)s / %(r)s'

    # SR: Simple ratio NIR/Red reflectance ratio (Jordan, 1969)
    sr_expr = '%(outpref)s_sr =1.0* %(nir)s / %(r)s'

    # SRc: Corrected Simple Ratio (Brown et al. 2000)
    src_expr = '%(outpref)s_src =1.0* $sr *(1-((%(mir)s -
%(minmir)s)/(%(maxmir)s - %(minmir)s)))'

    # MSR: Modified Simple Ratio (Chen, 1996)
    msr_expr = '%(outpref)s_msr =1.0* (%(nir)s / %(r)s -1)/(sqrt(%(nir)s /
%(r)s)+1)'

    # RGR: Red Green Ratio (Gamon and Surfus)
    rgr_expr = '%(outpref)s_rgr =1.0* %(r)s / %(g)s'

    # RGI: Red Green Index (Coops et al.)
    rgi_expr = '%(outpref)s_rgi =1.0* (%(g)s - %(r)s)/(%(g)s + %(r)s)'

    # NDVI: Normalized Difference Vegetation Index (Rouse et al., 1974)
    ndvi_expr = '%(outpref)s_ndvi =1.0* (%(nir)s - %(r)s)/(%(nir)s + %(r)s)'

    # NDVIc: Corrected NDVI (Nemani et al., 1993)
    ndvic_expr = '%(outpref)s_ndvic =1.0* $ndvi *(1-((%(mir)s -
%(minmir)s)/(%(maxmir)s - %(minmir)s)))'

    # GNDVIgreen: NGreen Normalized Difference Vegetation Index (Gitelson et
al., 1996)
    gndvi_expr = '%(outpref)s_gndvi =1.0* (%(nir)s - %(g)s)/(%(nir)s + %(g)s)'

    # NDWI: Normalized Difference Water Index (Gao, 1996)
    ndwi_expr = '%(outpref)s_ndwi =1.0* (%(nir)s - %(mir)s)/(%(nir)s +
%(mir)s)'

    # SLAVI: Specific Leaf Area Vegetation Index (Lymburner et al., 2000)
    slavi_expr = '%(outpref)s_slavi =1.0* %(nir)s /(%(r)s + %(mir)s)'

    # NCI: Normalized Canopy Index (Vescovo & Gianelle, 2008)
    nci_expr = '%(outpref)s_nci =1.0* (%(mir)s - %(g)s)/(%(mir)s + %(g)s)'

    # NBR: Normalized Burn Ratio -> NOT IMPLEMENTED
    # fire/burn index, use TM7/OLI_SWIR2

    # TCA: Tasselled Cap Angle (Powell et al., 2010; Gomez et al., 2011)
    tca_expr = '%(outpref)s_tca =1.0* atan(%(gr)s / %(br)s)' #deg angle

    # ln(-We)
    lnmwe_expr = '%(outpref)s_lnmwe =1.0* log(-%(we)s)'


    # MAIN
    landname= options['band_prefix'] #'toare_B'
```

```
indicespref= options['indices_prefix'] #'spectral'

#remove path before names and anything aftre the last point (ext)
#landpref=os.path.splitext(os.path.basename(landname))[0]

#remove ending numer from basename (purge path and @mapset)
#BASH: echo $(basename $landname) | sed 's/[0-9]*$//'
landpref=re.sub('[0-9]*$', '',os.path.basename(landname.split('@')[0]))

# define bands maps
if flags['o']:
    #landsat8
    g.message("OLI sensor")
    blue=landpref+'2'
    green=landpref+'3'
    red=landpref+'4'
    ninfrar=landpref+'5'
    minfrar=landpref+'7' #SWIR1
elif flags['t']:
    #landsat7
    g.message("TM/ETM+ sensor")
    blue=landpref+'1'
    green=landpref+'2'
    red=landpref+'3'
    ninfrar=landpref+'4'
    minfrar=landpref+'5'
else:
    #landsat8
    g.message("Warning: no sensor specified, defaout OLI used")
    blue=landpref+'2'
    green=landpref+'3'
    red=landpref+'4'
    ninfrar=landpref+'5'
    minfrar=landpref+'7' #SWIR1

#set region on a band map (are all equal)
g.run_command('g.region', rast = minfrar)

# mir max and min
min_mir = g.raster_info(minfrar)['min']
max_mir = g.raster_info(minfrar)['max']

bands= {
    "outpref" : indicespref,
    "b" : blue,
    "g" : green,
    "r" : red,
    "nir" : ninfrar,
    "mir" : minfrar,
    "minmir" : min_mir,
    "maxmir" : max_mir,
}

# compute indices with GRASS mapcalc
g.message("Calculating vegetation indices")
g.mapcalc(rr_expr % bands, overwrite = True)
g.mapcalc(sr_expr % bands, overwrite = True)
g.mapcalc(src_expr % bands, sr=indicespref+'_sr', overwrite = True)
g.mapcalc(msr_expr % bands, overwrite = True)
g.mapcalc(rgr_expr % bands, overwrite = True)
```

```
    g.mapcalc(rgi_expr % bands, overwrite = True)
    g.mapcalc(ndvi_expr % bands, overwrite = True)
    g.mapcalc(ndvic_expr % bands, ndvi=indicespref+'_ndvi', overwrite = True)
    g.mapcalc(gndvi_expr % bands, overwrite = True)
    g.mapcalc(ndwi_expr % bands, overwrite = True)
    g.mapcalc(slavi_expr % bands, overwrite = True)
    g.mapcalc(nci_expr % bands, overwrite = True)

    if flags['c']:
        tcname= options['tc_prefix']
        if tcname=="":
            g.message("Warning: no TC prefix, defaout 'tct8_C.' used")
            tcpref='tct8_C.'
        else:
            tcpref=re.sub('[0-9]*$',
'',os.path.basename(tcname.split('@')[0]))

        comp= {
            "outpref" : indicespref,
            "br" : tcpref+'1',
            "gr" : tcpref+'2',
            "we" : tcpref+'3',
        }

        g.message("Calculating Cap Tassellation indices")
        g.mapcalc(tca_expr % comp, overwrite = True)
        #g.mapcalc(lnmwe_expr % comp, overwrite = True) #null() 4 We>0

    return 0
    #End main


if __name__ == "__main__":
    options, flags = g.parser()
    sys.exit(main())
```